Cosmological simulations of the first galaxies

Latif, M. A.

Chapter 3

Lyman alpha emission from the first galaxies: Signatures of accretion and infall in the presence of line trapping*

The formation of the first galaxies is accompanied by large accretion flows and virialization shocks, during which the gas is shock-heated to temperatures of $\sim 10^4$ K, leading to potentially strong fluxes in the Lyman alpha line. Indeed, a number of Lyman alpha blobs has been detected at high redshift. In this letter, we explore the origin of such Lyman alpha emission using cosmological hydrodynamical simulations that include a detailed model of atomic hydrogen as a multi-level atom and the effects of line trapping with the adaptive mesh refinement code FLASH. We see that baryons fall into the center of a halo through cold streams of gas, giving rise to a Lyman alpha luminosity of at least 10^{44} erg s^{-1} at $z = 4.7$, similar to observed Lyman alpha blobs. We find that a Lyman alpha flux of 5.0×10^{-17}erg cm^{-2} s^{-1} emerges from the envelope of the halo rather than its center, where the photons are efficiently trapped. Such emission can be probed in detail with the upcoming James Webb Space Telescope (JWST) and will constitute an important probe of gas infall and accretion.

*Originally published as: Latif, M. A., Dominik R.G. Schleicher, Spaans M., Zaroubi S., Monthly Notices of the Royal Astronomical Society: Letters, Volume 413, Issue 1, pp. L33-L37(2011).

3.1 Introduction

Early-type galaxies are known to produce copious Lyman alpha photons due to their spatially extended gas distribution. In protogalactic halos gas transfers its gravitational binding energy to the excitation of hydrogen atoms which results in Lyman alpha emission (Haiman et al. 2000b; Dijkstra et al. 2006a,b). Therefore, the gas in dark matter halos exceeding a virial temperature of $\sim 10^4$ K may be detected in the Lyman alpha line emission. The presence of ionizing radiation sources may enhance the Lyman alpha flux as gas is photo-ionized, and and supernova feedback may further increase the escape fraction by generating a more clumpy structure. These ionization sources could be the first stars or mini-quasars. A luminous quasar can boost the emission of Lyman alpha photons by several orders of magnitude Haiman & Rees (2001).

Many Lyman alpha blobs (LABs) have been observed at high redshift (Yang et al. 2009; Ouchi et al. 2009; Matsuda et al. 2004; Steidel et al. 2000). In the light of recent detections at redshift > 7 (Lehnert et al. 2010; Vanzella et al. 2010), it is of high interest to understand what drives the emission and how it is spatially distributed. A number of LABs have been observed whose most probable origin is cold accretion of gas onto dark matter halos (Nilsson et al. 2006; Smith & Jarvis 2007).

Numerical simulations show that cooling by Lyman alpha radiation induces collapse in protogalactic halos. Moreover, baryons accumulate into the center of halos by penetration of cold streams of gas through the shock heated medium (Fardal et al. 2001; Wise et al. 2008; Jappsen et al. 2009; Regan & Haehnelt 2009a; Dekel et al. 2009; Kereš et al. 2009; Goerdt et al. 2010; Latif et al. 2010; Shang et al. 2010). Cold streams with temperatures of $\sim 10^4$ K could be potential sources of spatially extended Lyman alpha emission (Dijkstra & Loeb 2009a). Johnson et al. (2010) found that Lyman alpha radiation can also be emitted during accretion of gas on black holes formed by direct collapse in the first galaxies. Such emission is potentially detectable with JWST[†]. Similarly, it allows to probe the starburst component through the enhanced emission in several recombination lines (Johnson et al. 2009).

The presence of large columns of neutral hydrogen gas causes the trapping of Lyman alpha photons (Spaans & Silk 2006; Latif et al. 2010; Schleicher et al. 2010b), which was neglected in some of the previous studies. In this letter, we aim at a self-consistent modeling of Lyman alpha emission driven by accretion flows, including dynamics, non-equilibrium chemistry of H, H^+, He, He^+ and He^{++}, detailed level populations of atomic hydrogen, as well as the trapping of hydrogen line photons due to large column densities. The prime objective of this work is to study the origin and spatial distribution of Lyman alpha emission, which is detectable with JWST.

3.2 Modeling of the physics

For our simulations, we employ an extended version of the adaptive mesh refinement (AMR) hydrodynamics code FLASH (Dubey et al. 2009). FLASH is a module based Eulerian grid parallel simulations code. We use an AMR grid to achieve high dynamic resolution in the regions of interest. We employ the directionally split

[†]http://www.stsci.edu/jwst/instruments/nirspec/sensitivity

piece wise parabolic method (PPM) for hydrodynamic calculations, which is an improved form of the Godunov method (Colella & Woodward 1984). This method is well suited for flows involving shocks and contact discontinuities. The dark matter is simulated based on the particle mesh (PM) method. In order to create Gaussian random field initial conditions, we run the COSMICS package developed by Bertschinger (1995). We start our simulation at redshift 100. Our computational periodic box has a comoving size of 10 Mpc. We perform our simulations in accordance to the ΛCDM model with WMAP 5-year parameters. We select a 4×10^9 $M_\odot$ halo at redshift 7 and follow its collapse. We enforce 8 additional levels of refinement, which gives 15 levels of refinement in total. In this way, we obtain a dynamic resolution limit of 70 pc (comoving), and can still follow the further evolution until redshift $z = 4.7$. We impose the Truelove criterion by refining according to the Jeans length (Truelove et al. 1997). We resolve the Jeans length by at least 20 cells.Such resolution was shown to be sufficient for accurately resolving turbulent structures during gravitational collapse (Federrath et al. 2010). When the highest refinement level is reached, we prevent artificial fragmentation via Jeans-heating. We assume a primordial gas composition with 75% hydrogen and 25% helium by mass.

We have developed a chemical network for the non-equilibrium modeling of non-molecular species. For this purpose, we solve the rate equations of the following species H, H^+, He, He^+, He^{++} and e^- for non-equilibrium ionization. The rate equations for these species are solved using the backward difference formula (BDF) method of Anninos et al. (1997). We adopt the chemical rates of Abel et al. (1997) and Schleicher et al. (2008b). We further solve for the level populations of atomic hydrogen up to the fifth electronically excited state, and model the non-equilibrium cooling including hydrogen line emission, collisional ionization cooling, recombination cooling, Bremsstrahlung cooling and Compton cooling/heating. The transition rates for the level populations are based on work of Omukai (2001). At an optical depth $\tau_0 > 10^7$, the photon escape time becomes longer than the gas free fall time. Because of the weak dependence of the photon escape time on the gas number density, $t_{ph} \propto n^{-1/9}$, trapping becomes important important during the collapse since the latter scales as $n^{-1/2}$. A detailed discussion of such line trapping effects is given by Omukai (2001); Spaans & Silk (2006); Schleicher et al. (2010b). We have computed the Lyman alpha luminosity by determining the Lyman alpha emissivity and integrating it over the virial volume of a halo. Further details of the luminosity and flux calculation can be found in Dijkstra et al. (2006a).

3.3 Results and Conclusions

The initial density perturbations decouple from the Hubble flow and begin to collapse via gravitational instabilities. The gas is shock-heated during the non-linear collapse of density perturbations. At redshift 10, the halo begins to virialize. In the process of virialization, part of its gravitational energy is converted into thermal energy. This heats up the gas and results in the emission of Lyman alpha photons. The gas is accreted into the center of the halo through cold streams of $\sim 10^4$ K as shown in figure 3.1. The upper panels of figure 3.1 show the density at different redshifts while lower panels show corresponding temperatures. Typical number densities of

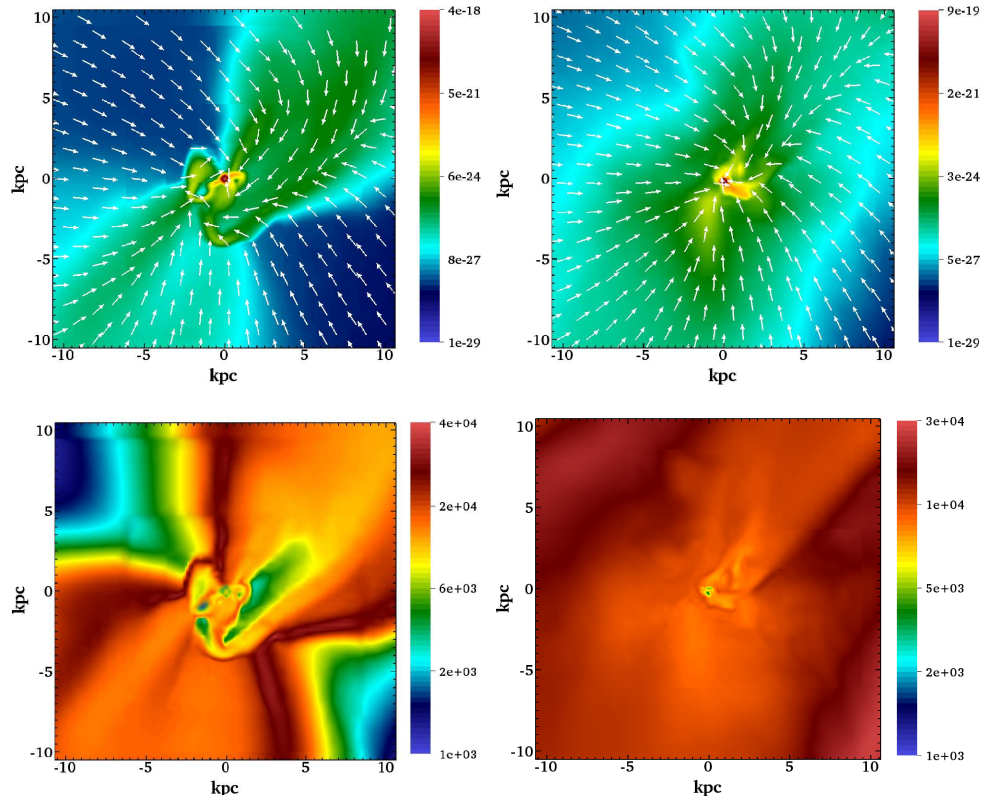

Figure 3.1: The upper panels of this figure show the density slices through the center of the halo. The left panel is for redshift 4.7 and right panel for redshift 8. Velocity vectors are overplotted on the density slices. The bottom two panels show the corresponding temperatures. The figure shows the inner region of 20 kpc in comoving units.

the cold streams are of the order of 0.01-1 cm^{-3}. Density and temperature radial profiles are depicted in the upper left and right panels of figure 3.2. We see that in the presence of hydrogen line emission the gas cools isothermally. The density profile of the halo is $\sim r^{-2.3}$, which agrees with results of Wise et al. (2008). The ionization degree of the gas is shown in the bottom left panel (HII abundance) of figure 3.2. We see that most of the gas remains neutral at 10^4 K, ionized fraction goes down due to faster recombination at higher densities $\sim n^{-0.5}$. The gas radial velocity is depicted in the bottom right panel of figure 3.2. It can be seen from the figure that gas is falling into the center of the halo. The velocity profile also shows that gas is accreted onto the halo through accretion shocks. The cold streams have typical column densities of about 10^{19} cm^{-2}. A radial profile of the column density is shown in figure 3.3. At columns above 10^{21} cm^{-2} the gas optical depth exceeds 10^7 and Lyman alpha trapping becomes effective. The Lyman alpha emissivity is shown in figure 3.3. It can be seen from the figure that above columns of the order of 10^{22} cm^{-2}, Lyman alpha photons are trapped and cooling through this line is completely suppressed. That is

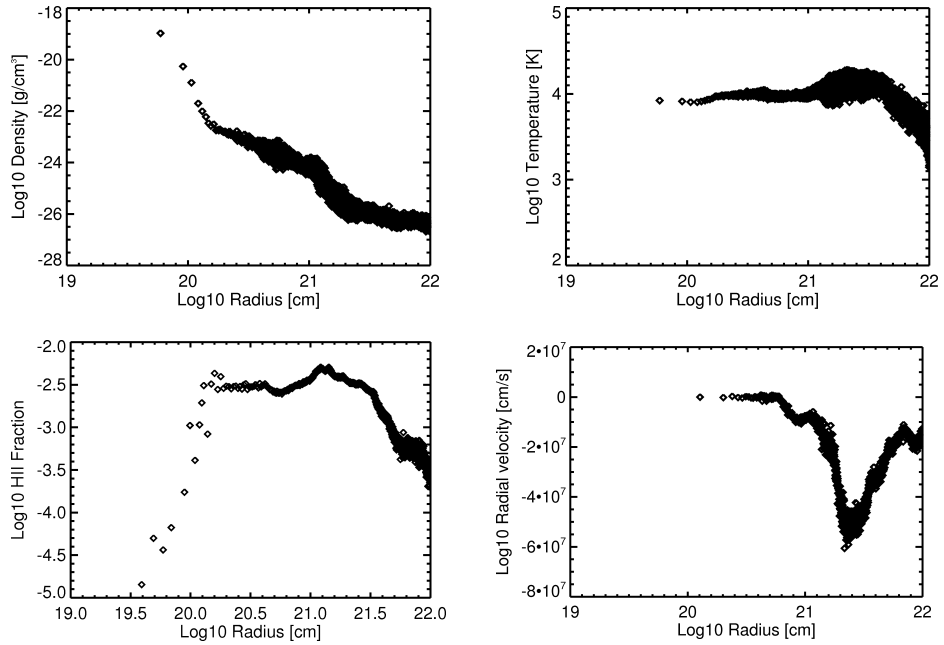

Figure 3.2: All panels in this figure are log log plots. The upper left panel shows the radial density profile of the halo. The radial temperature profile for the halo is depicted in the upper right panel. HII abundance is shown in the lower left panel. The radial velocity of the halo is depicted in the lower right panel.

why the Lyman alpha emissivity sharply declines in figure 3.3. We explored the local density variations and found that the maximum variation of the column density does not exceed an order of magnitude. In this sense, our calculation should provide a conservative lower limit on the expected flux. In the presence of Lyman alpha trapping, cooling can proceed through higher electronic states of atomic hydrogen (Schleicher et al. 2010b). For comparison, the total emissivity from higher states of atomic hydrogen and recombination/Bremsstrahlung processes is shown in figure 3.3. The total emissivity plot shows that despite line trapping, cooling still proceeds through these higher states of atomic hydrogen, particularly through 2s-1s and 3-2 transitions, and the thermal evolution is approximately isothermal.

The radial profile of the enclosed Lyman alpha luminosity is shown in figure 3.3. If the emission originates preferentially from the center, an approximately flat profile would be expected, while for uniform emission, a power-law behavior as $\sim r^3$ would be expected due to volume effects. Here, we find the absence of emission in the central core, then a sharp increase in luminosity between radii of $10^{20.2}$ cm $- 10^{21}$ cm by four orders of magnitude, and a more modest increase between radii of 10^{21} cm $- 10^{22}$ cm. This behavior reflects the generation of Lyman alpha emission through accretion shocks. JWST can confirm the presence of such a brightness profile. The total Lyman alpha luminosity from the halo is 10^{44} erg s^{-1}, which is consistent with observed Lyman alpha blobs (Ouchi et al. 2009; Goerdt et al. 2010).

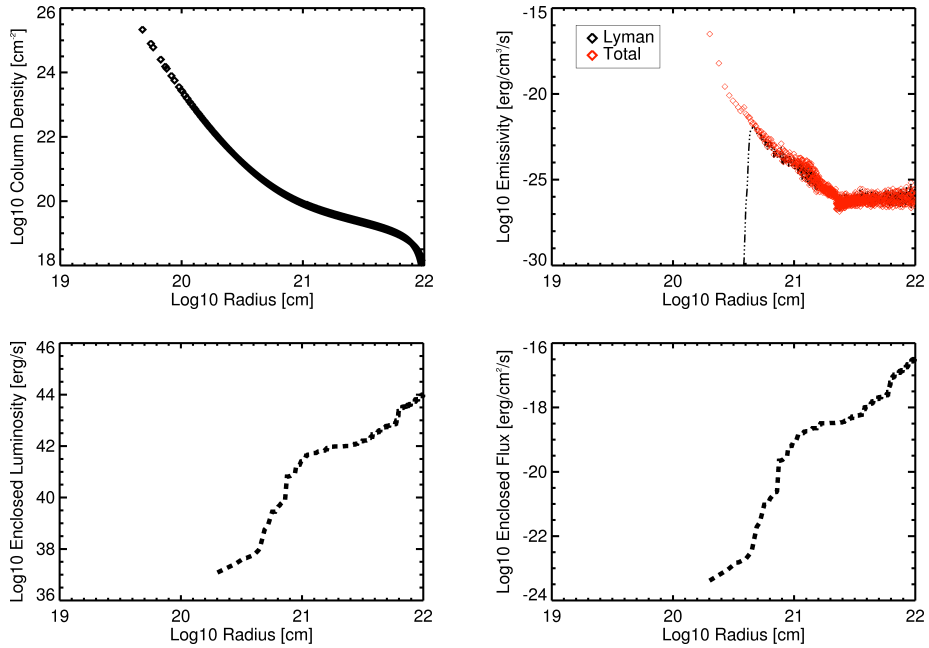

Figure 3.3: All panels in this figure are log log plots. The upper left panel shows column density plotted against the radius of the halo. Lyman alpha emissivity radial profile emerging from the halo is shown in the upper right panel. Lyman alpha luminosity is shown in the lower left panel. Lyman alpha flux is plotted against the radius of the halo in the lower right panel.

The emerging flux from the halo is depicted in figure 3.3. We find a total flux of 5.0×10^{-17}erg cm^{-2} s^{-1}. At redshift 4.7, the observed Lyman alpha wavelength is at 0.68 microns. This can be detected with the JWST-instrument NIRSpec for integration times of 10^4s, with S/N=10 and R=100. JWST spectrograph NIRSpec will have angular resolution of 0.1 arc-sec for 2 micron, and NIRcam will be well-suited for higher angular resolution with field of view of 2.2x2.2 arcmin^2 and 4096^2 pixels for shorter wavelength of 0.6-2.3 micro meter. The halo in our case will have an angular size of 0.5 arc-sec at redshift 4.7. It should be detectable with NIRcam/NIRSpec. For extended emission of Lyman alpha, it may need higher integration time ($\sim 10^5$ sec) to resolve the flux from extended sources. The total mass of our halo at redshift 4.7 is 2×10^{10} M$_\odot$, which is not extreme in any way. Selecting higher mass halos will produce higher fluxes as there is a power law relation between the mass of a halo and its luminosity $L_{Ly\alpha} \propto M^{5/3}$ (Dekel et al. 2009; Dijkstra et al. 2006a). We stopped our simulation at a redshift of 4.7 as it becomes computationally too expensive to follow the further time evolution.

In this work, we assume that there is no X-ray/UV background flux. Its presence can heat the gas and may increase the Lyman alpha flux (Spaans & Meijerink 2008; Zaroubi et al. 2007). We have compared our results with (Dijkstra et al. 2006a) and found good agreement. We have assumed here that the halo is metal free. The addi-

tion of small amounts of dust can absorb Lyman alpha photons efficiently, unless the gas is inhomogeneous (Haiman & Spaans 1999). However, in-falling gas may still be pristine for isolated halos. We have ignored H_2 cooling, which is suppressed in the presence of a strong UV background ($J_{21} > 100$) (Dijkstra et al. 2004; Cazaux & Spaans 2009). Shang et al. (2010) found that even $J_{21} \sim 30$ will be sufficient to quench H_2 formation for local variations in flux see Dijkstra et al. (2008). At higher redshifts, it is possible that H_2 may form for more modest radiation backgrounds. Even then, we expect H_2 formation preferentially at the center of the halo, while the accretion at the virial radius may still include a gas phase at 10^4 K. This supports our main conclusion that Lyman alpha radiation originates mostly from gas in halo envelope.

Some LABs are also associated with massive star forming galaxies (Matsuda et al. 2006) where stellar feedback or an AGN could power Lyman alpha radiation. It is clear that starbursts and AGNs are also potential candidates to power or enhance the observed Lyman alpha luminosities. It is not fully clear if our results are also applicable to such situations, although we expect similar effects of line trapping in the centers of such galaxies if $N_H/\Delta v \geq 10^{21}$ cm^{-2} km^{-1} s, with Δv the cumulative velocity difference along the atomic hydrogen column N_H. Current modeling uncertainties concern both the star formation efficiency and the initial mass function. Both radiative feedback, leading to the formation of HII regions, as well as mechanical feedback, providing a more clumpy structure with higher escape fractions, need to be modeled self-consistently. Outflows if present may enhance the detectability of Lyman alpha emission in the outskirt of the halo, 5% of the emitted Lyman alpha photons could be directly transmitted to the observer along the line of sight (Dijkstra & Wyithe 2010). In the future, cosmological radiative transfer simulations including feedback effects should be performed to obtain more robust results.

3.4 Acknowledgments

The FLASH code was in part developed by the DOE-supported Alliance Center for Astrophysical Thermonuclear Flashes (ACS) at the University of Chicago. DRGS acknowledges funding via the European Communitys Seventh Framework Programme (FP7/2007-2013) under grant agreement No. 229517 and via HPC-EUROPA2 (project number: 228398) with the support of the European Commission Capacities AreaResearch Infrastructures Initiative. SZ thanks the lady Davis foundation for support. We thank the anonymous referee for a careful reading of the manuscript and many insightful comments.